STRUCTURAL CONTROL AND HEALTH MONITORING
Struct. Control Health Monit. (2012)
Published online in Wiley Online Library (wileyonlinelibrary.com). DOI: 10.1002/stc.1532

Feasibility of displacement monitoring using low-cost GPS receivers

Hongki Jo[1], Sung-Han Sim[2], Andrzej Tatkowski[1], B. F. Spencer Jr.[1,*,†] and Mark E. Nelson[3]

[1]*Department of Civil and Environmental Engineering, University of Illinois at Urbana-Champaign, Urbana, IL 61801 USA*
[2]*School of Urban and Environmental Engineering, UNIST, Ulsan 698-798, Korea*
[3]*Department of Molecular and Integrative Physiology and the Beckman Institute for Advanced Science and Technology, University of Illinois at Urbana-Champaign, Urbana, IL 61801 USA*

SUMMARY

Many of the available SHM approaches neither readily support displacement monitoring nor work in concert with one another to take advantage of displacement-based SHM for various long-period structures. Although survey-quality GPS technology offers the possibility of measuring such displacements with sub-centimeter precision, the associated cost is too high to allow for routine deployment. Low-cost GPS chips commonly found in mobile phones and automobile navigation equipment are attractive in terms of size, cost, and power consumption; however, the displacement accuracy of these GPS chips is on the order of several meters, which is insufficient for SHM applications. Inspired by sensory information processing strategies of weakly electric fish, this paper investigates the potential for using dense arrays of relatively low-precision GPS sensors to achieve high-precision displacement estimates. Results show that dynamic response resolution as low as 20–30 cm can be achieved and that the resolution improves with the number of sensors used. Copyright © 2012 John Wiley & Sons, Ltd.

Received 26 October 2011; Revised 25 September 2012; Accepted 5 October 2012

KEY WORDS: structural health monitoring, wireless smart sensor network, GPS, low cost, displacement monitoring

1. INTRODUCTION

Recent catastrophic structural failures have focused public attention on the declining state of aging civil infrastructure and the necessity for SHM. The research community has turned to wireless smart sensor networks (WSSNs) to develop approaches for continuously monitoring the health of essential infrastructure, both old and new, because WSSNs offer many attractive features, such as ease of installation, wireless communication, on-board computation, battery power, relatively low cost, and small size. Indeed, SHM using wireless smart sensor technology has emerged as a promising solution that will reduce inspection costs, optimize repairs, and ensure public safety as building and bridge structures become higher, longer, and more complex. Recent successful implementations of WSSN for full-scale SHM systems have demonstrated the practical use of the technology [1–4].

However, most current SHM approaches using WSSN, even using traditional wired systems, rarely support displacement monitoring, primarily because of the difficulty in measuring absolute displacements. Many of the advantages of displacement-based SHM for long-period structures such as high-rise buildings and cable-supported bridges are left untapped.

GPS technologies are able to provide absolute displacement measurements. A state-of-the-art real-time kinematic (RTK) technique with dual-frequency GPS receivers that can use L1/L2 carrier phases allows sub-centimeter accuracy. The number of studies for validating the accuracy and feasibility of

*Correspondence to: B.F. Spencer, Jr., Department of Civil and Environmental Engineering, University of Illinois at Urbana-Champaign, Urbana, IL 61801, USA.
†E-mail: bfs@illinois.edu

such survey-level GPS technologies include but are not limited to those by Nickitopoulou *et al*. [5], Psimoulis *et al*. [6], Psimoulis and Stiros [7], and Casciati and Fuggini [8]. Such dual-frequency GPS system has been used for displacement monitoring of civil infrastructure by Ashkenazi *et al*. [9], Celebi *et al*. [10], Nakamura [11], Fujino *et al*. [12], Kijewsji-Correa *et al*. [13], Watson *et al*. [14], and Casciati and Fuggini [8]. An extensive review of recent research and applications of GPS-based monitoring technologies have been provided by Yi *et al*. [15]. However, this kind of dual-frequency GPS sensor is quite high in cost, making it unsuitable for dense deployments envisioned for damage detection.

Single-frequency GPS receivers are potentially suitable for dense deployments using smart sensors because of their small size, low cost, and relatively low power consumption. Displacement monitoring systems using the single-frequency low-cost GPS have been investigated in a number of studies. Knecht and Manetti [16] employed a low-cost L1 GPS for static displacement measurements, particularly, using the carrier phase signal. However, the high-cost and power consumption of the sophisticated antenna used to measure the L1 carrier phases do not fit the requirement of WSSN application. Saeki and Hori [17] and Saeki *et al*. [18] employed an inexpensive patch antenna to measure the carrier phases from the L1 GPS; however, their applications have been limited to only static displacement measurements. On the other hand, the feasibility of the L1 coarse/acquisition (C/A) code-based GPS system to SHM, which is generally used for navigation purposes, has not been reported in the literature, primarily because of the perceived low resolution of the low-cost GPS sensors (on the order of meters).

Mimicking biological signal processing strategies has tremendous potential for improving the quality of information obtained in WSSN applications. Inspiration for this work comes from weakly electric fish found in South America and Africa (Figure 1). These fish generate electrical fields using a specialized electric organ located in their tail region (black bar in the right of Figure 1) to actively probe their environment [19]. These fish emit millivolt-level electrical discharges and detect microvolt-level voltage perturbations arising from nearby objects in the water. This phenomenon is called electrolocation and is analogous to echolocation abilities found in bats and dolphins (see the right of Figure 1). The body of a weakly electric fish is covered with around 15,000 electroreceptors. Each individual electroreceptor, however, is a relatively low-resolution sensor and does not provide reliable event detection. To compensate for this, the nervous system of the electric fish creates arrays of virtual sensors with the desired resolution and sensitivity by pooling information from multiple low-resolution skin sensors. This approach allows the fish to detect and localize targets in 3D space and assess target characteristics such as size, shape, and electrical impedance. This suggests the possibility of designing a WSSN that achieves high-precision displacement measurements using a dense array of low-cost L1 C/A code-based GPS sensors.

This study investigates the potential for using low-cost L1 C/A code-based GPS sensors to obtain displacement measurements suitable for monitoring large civil infrastructure. The accuracy of low-cost GPS modules is assessed through various static and dynamic tests and through analyzing the correlation characteristics of the noise in the GPS signals. Analytical studies are also considered to assess the potential of using dense arrays of such GPS sensors, based on the experimental results.

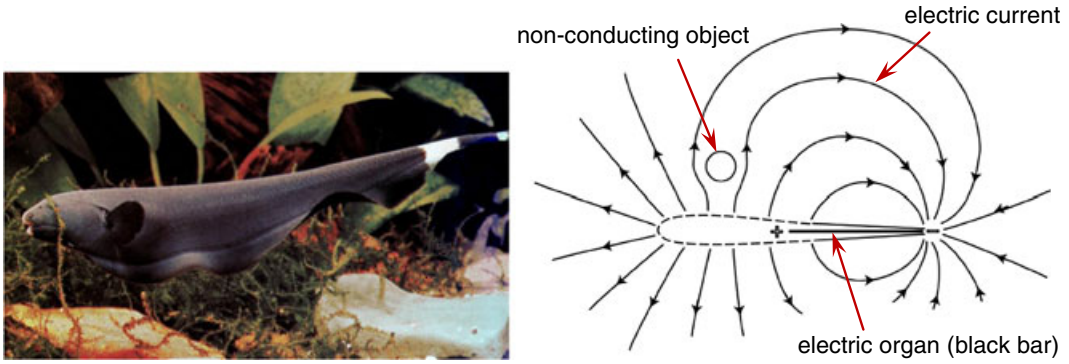

Figure 1. Weakly electric fish (left) and principal of electrolocation (right) [19].

DOI: 10.1002/stc

2. COARSE/ACQUISITION CODE-BASED LOW-COST GPS RECEIVERS

2.1. GPS signals and frequencies

A GPS satellite broadcasts a navigation message at a rate of 50 bps. Each message contains the satellite clock, satellite location, and status of the satellite. The messages are encoded using code division multiple access, allowing messages from individual satellites to be distinguished from one another on the basis of unique encodings for each satellite. Two distinct types of code division multiple access encodings are used: C/A code, which is freely available to the public, and the precise (P) code, which is usually reserved for military applications. All satellites broadcast at the same two frequencies: one at 1575.42 MHz (10.23 MHz $\times$ 154), called the L1 carrier, and second at 1227.6 MHz (10.23 MHz $\times$ 120), called the L2 carrier. The C/A code is transmitted on the L1 carrier at 1.023 MHz, and the P code is transmitted on the both L1 and L2 carriers at 10.23 MHz, but 90° out of phase with C/A code on the L1. Figure 2 shows the modulation scheme of GPS signals.

2.2. GPS receiver types

There are two different types of GPS receivers in terms of frequency usage; one is the single-frequency (L1) C/A code-based GPS receiver, which is usually used for navigation purposes, and the other one is the dual-frequency (L1 and L2) carrier-phase-based GPS receiver. The accuracy of receivers is generally a function of the ability of the receivers' electronics to accurately compare the signal sent from the satellite and an internally generated copy of the same signal within the receiver. It is by using the time delay between the GPS signal and the receiver's signal that the distance from the satellite can be calculated. Considering the wavelengths of the C/A code ($(3 \times 10^8$ m/s)/1.023×10^6 Hz = 293.3 m) and the L1 carrier ($(3 \times 10^8$ m/s)/1575.42×10^6 Hz = 0.190 m), even a 1% alignment error, for instance, can cause 2.933 m of error for single-frequency GPS and 1.9 mm of error for dual-frequency GPS. Assuming the same alignment error, the accuracy of the dual-frequency GPS receiver that uses both the L1 and L2 carriers with frequencies 1575.42 and 1227.6 MHz will be about 1500 times better than the single-frequency GPS receiver using C/A code with a frequency of 1.023 MHz. Of course, effects other than alignment error can introduce additional errors. The overall accuracy of GPS receivers is at the meters level for single-frequency GPS receivers and at the centimeters level for dual-frequency GPS receivers.

Dual-frequency GPS systems have been widely used for displacement monitoring purposes because of their high accuracy (Figure 3). The RTK technique, which provides real-time correction using a differential GPS (DGPS) method, enables even millimeter level accuracy. However, because of high cost (typically tens of thousands of dollars per unit), only a small number of units can be deployed on a structure.

C/A code-based GPS receivers are cheap, small, and consume little power, which offer the potential for deploying a dense array of such sensors. However, the meters-level accuracy is still insufficient for SHM applications. As a result, neither the use nor the feasibility of using low-cost C/A code-based GPS receivers for SHM applications has been reported to date.

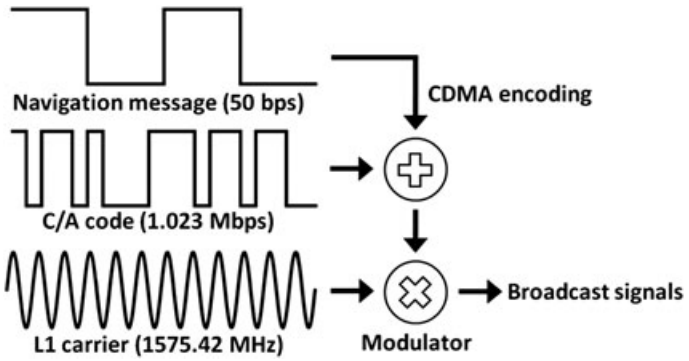

Figure 2. GPS signal modulation scheme [29].

DOI: 10.1002/stc

Figure 3. Leica GMX902 dual-frequency GPS receiver (left) and AX1202 antenna (right): 0.2 mm RMS accuracy, 2.4 W power consumption, and up to 20 Hz sampling rate [30].

2.3. MT3329 GPS chipset (C/A code-based single-frequency GPS module)

Recently, GlobalTop has released a new high-sensitivity and low-power GPS module (Gms-u1LP; Figure 4). It uses the MediaTek MT3329 GPS chipset (L1 frequency, C/A code, 66 channels), consumes only 24 mA at 3.3 V, contains an integrated ceramic antenna, features −162 dBm of sensitivity, has 3.0 m root mean square (RMS) of position accuracy, and is relatively small ($16 \times 16 \times 6$ mm). Also, it supports sampling rates up to 10 Hz and costs only about $20 per unit. Moreover, it comes with customizable software, which allows sampling rate change, power saving mode, binary protocol, data logging function, assisted GPS, and so on (http://www.gtop-tech.com), although some core algorithms cannot be accessed. These characteristics offer the potential for implementation in a WSSN.

3. PRELIMINARY GPS TESTING

To assess the feasibility of low-cost GPS receivers for SHM applications, the achievable accuracy and limitations of the GPS need to be identified. Casciati and Fuggini [20] have provided a well-organized test procedure for GPS performance calibration. On the basis of the calibration procedure, this study extensively investigates the performance of the low-cost single-frequency GPS for both static and dynamic conditions in time and frequency domains.

3.1. Experiment set-up

For the preliminary investigation, four GlobalTop Gms-u1LP GPS modules [31] with the integrated ceramic antennas were used. The four GPS receivers were placed together on a small wooden plate, and FTDI cables were used to convert UART (TTL) serial data from the GPS receivers to USB signals, which were then transmitted to a laptop computer. The GPS data, in NMEA 0183 format, is recorded through the HyperTerminal program included in Microsoft Windows XP. Static and dynamic tests were performed on the roof of the Newmark Civil Engineering Laboratory (NCEL) building located in the University of Illinois at Urbana-Champaign campus. Even though there were several small steel chimneys, about 30 cm in diameter and 2 m in height, the roof provided a quite open field environment, free from other buildings that may obstruct the view of low elevation satellites.

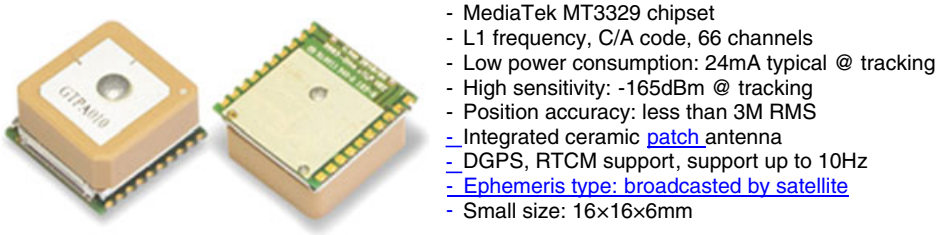

Figure 4. Gms-u1LP single-frequency GPS module with integrated antenna [31].

DOI: 10.1002/stc

3.2. Static tests

Static calibration tests were carried out to assess the variation in the static measurements over time and the possibility of using the DGPS concept with low-cost single-frequency GPS receivers. Additionally, these tests were executed to quantify the background noise characteristics in actual GPS measurements on a structure. These four GPS receivers were placed at a fixed location on the roof of the NCEL building, and four consecutive days of data, from March 1–4, 2011, were measured at a 1 Hz sampling rate. All the four GPS modules were attached on a plastic plate in the same direction, and the plate and a laptop were wrapped with thin plastic cover to protect them from possible environmental effects. The first 3 days were sunny with no clouds, and the last day was rainy with weak thunderstorm conditions in the Champaign-Urbana area.

Data, from 07:00 PM on the first day to 07:00 PM on the next day (i.e., 24 h), are plotted in Figure 5; the left column compares measurements from a single GPS receiver across 4 days, and the right column compares readings from four GPS receivers on a single day.

As shown in the left column of Figure 5, very strong correlation was found between the static data for the first 3 days for GPS-1, whereas the data for the fourth day deviated significantly from the previous three. Considering that the orbital period of GPS satellites is 12 h and the multipath distortion would be repeated every orbital period, the correlated static noises can be predicted and subtracted from the actual structural measurements in the future. However, the elimination of the repeated noise seems to be valid only for days with clear skies; the static data measured in the rainy day (day 4) were quite different from the other 3 days' data. Weather is not known to affect on GPS signal. Instead, standing water on GPS antenna is problematic [21]; water drops or thin layer of water standing on the plastic film that covered the GPS modules and laptop may have caused the signal distortion during the rainy day.

To utilize DGPS technique, which can be realized with a correction signal from a reference GPS station placed at a fixed location, the reference and mobile GPS modules need to be assumed to have the same amount of static noise. However, even on a sunny day, the static noises among the four different GPS modules did not show strong correlation (Figure 5, right column). Thus, the DGPS concept with low-cost GPS sensors does not appear to be useful in practice. Note that the dilution of

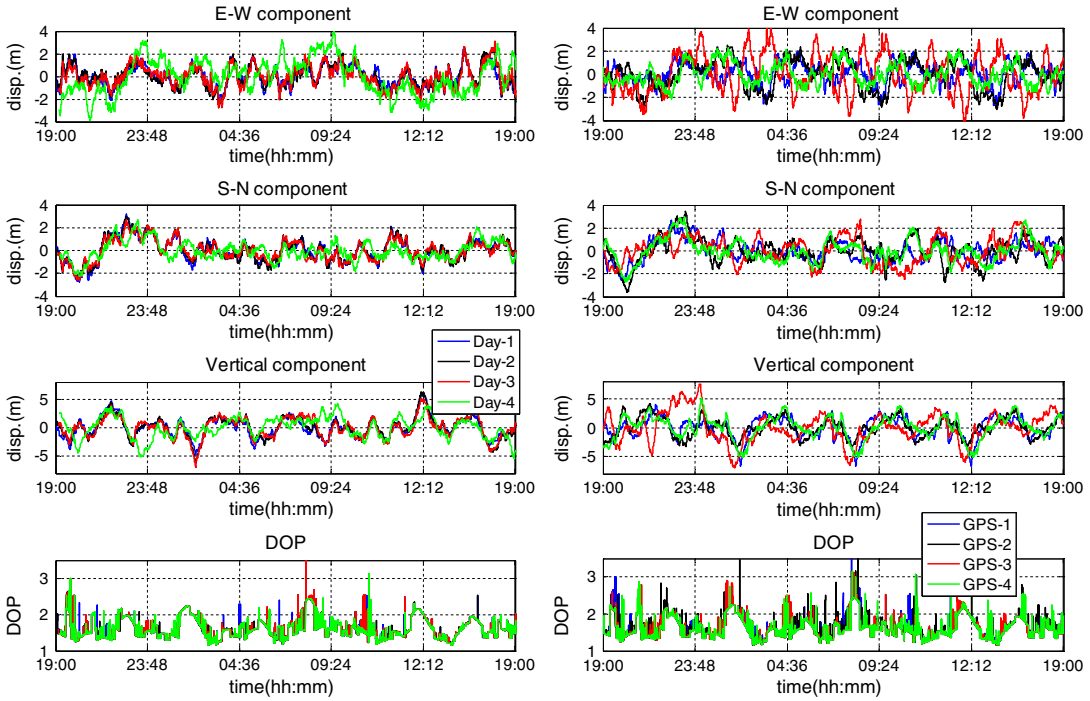

Figure 5. Static measurement comparisons: GPS-1 data for 4 days (left) and GPS 1–4 data for the third day (right).

DOI: 10.1002/stc

precision (DOP) data for all four GPS modules and for the 4 days showed a quite similar pattern over time. Considering the DOP values ranging over 1.2–3.0, the GPS satellite geometry condition was quite good at that time.

Figure 6 shows the correlation between the data from the first 2 days with clear skies in E/W, N/S, and vertical directions. The RMS value changes of the static measurements for all days are plotted in Figure 7. The RMS errors of the GPS modules, except GPS-3, for the first 3 sunny days' data were about 1 m and slightly increased for the rainy day measurement in the horizontal directions. In comparison with other GPS modules, GPS-3 showed larger RMS errors in the E/W and vertical directions, which may be attributed to the non-uniform hardware quality of the low-cost GPS modules; such larger RMS error is still in the acceptable deviation range of 3 m RMS specified in the datasheet of the GlobalTop Gms-u1LP module.

3.3. Dynamic tests

To check the applicability of low-cost GPS sensors to dynamic displacement measurements, calibration tests were performed. A horizontal rotor blade was constructed for the preliminary dynamic tests (Figure 8). A wooden plank, 2.0 m long and 0.3 m wide, was fixed on top of a DC gear motor having 1/8 HP and a maximum rotational speed of 33 RPM. When assembled, the device equivalently has two 1.0-m-long blades extending in opposite directions from the central motor. The four GlobalTop Gms-u1LP GPS sensors were placed together at the tip of the blades (1.0 m distance from the rotational center), and a laptop was used to power and receive data from the GPS sensors. The laptop was powered using a rechargeable car battery, and both the battery and the laptop were placed on the center of the wooden plank. Varied rotational speeds were tested to quantify the range of frequencies and amplitudes that could be successfully tracked using the low-cost single-frequency GPS sensors. A 5 Hz sampling rate was used for the dynamic tests; the day was sunny during the dynamic tests.

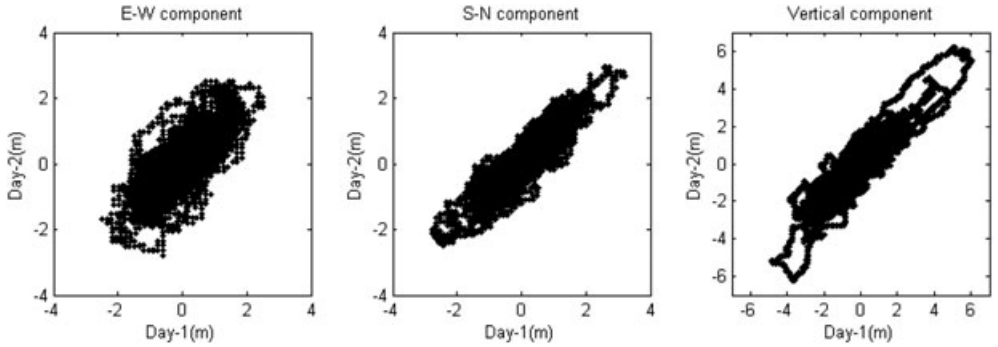

Figure 6. Correlation between measurements on different days: E/W (left), S/N (middle), and vertical (right) components.

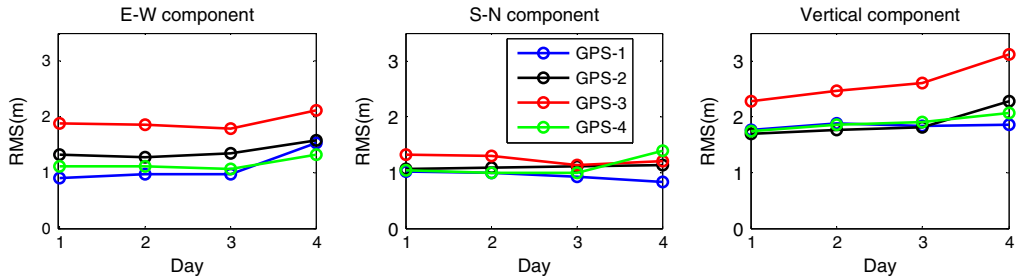

Figure 7. RMS value changes of static measurement over all days: E/W (left), S/N (middle), and vertical (right) components.

DOI: 10.1002/stc

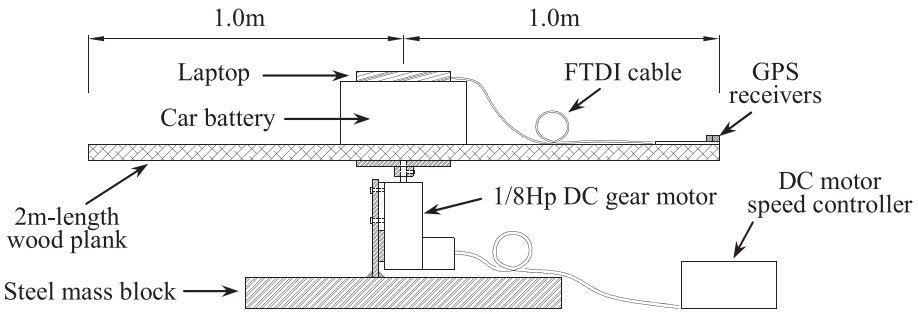

Figure 8. Rotor blade for GPS dynamic testing.

Figure 9 shows the time histories of 30 min of measurements in a circular motion at a 1.0 m radial distance with a 2.3 s rotational period for all four GPS modules. The simultaneous E/W and N/S components shown in the left diagram of Figure 9 seem not to provide any appearance of circular motion; they even seem to be contaminated with drifting noises of over ±5 m. However, clear sinusoidal waves were observed in each directional component of the 1-min detail plotted on the right in Figure 9. The GPS modules measured the dynamic movement well; nevertheless, some low-frequency drift errors are present.

The PSDs clearly showed the frequency contents of the time histories in Figure 10. The frequency of 0.43 Hz corresponding the rotor's rotational speed was shown in both E/W and N/S directions.

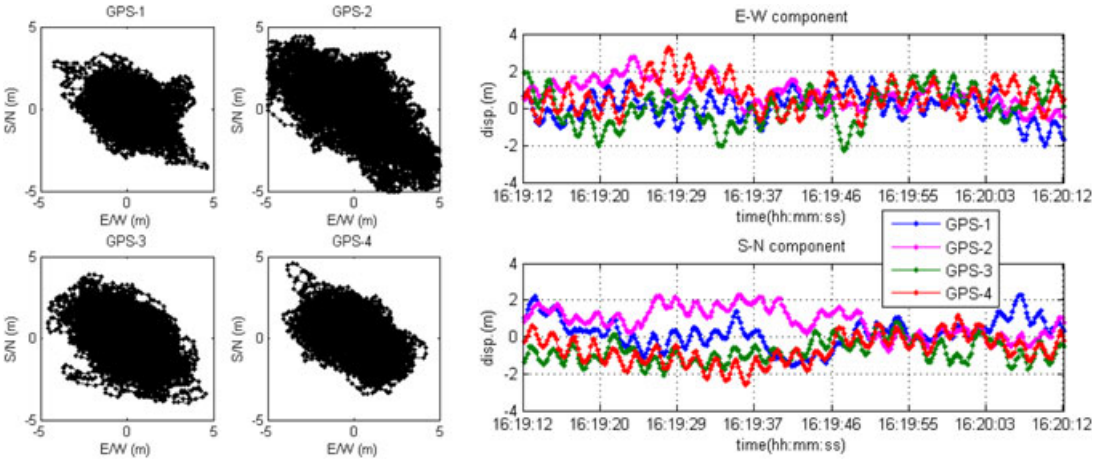

Figure 9. Dynamic measurements (1.0 m radius and 2.3 s period): 30-min data in both directions (left) and each directional component of 1-min data (right).

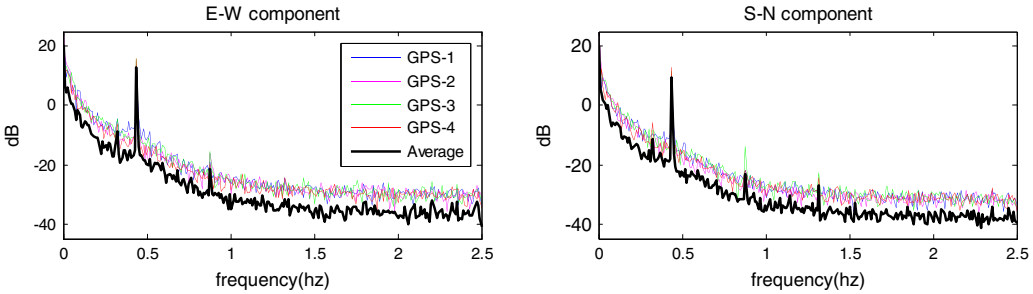

Figure 10. PSDs of the GPS measurements in E/W direction (left) and S/N direction (right): 1.0 m radius and 2.3 s period.

DOI: 10.1002/stc

However, unexpected additional peaks were observed around 0.86 and 1.29 Hz. These additional frequencies may be attributed to the quantization error of the GPS measurements, which can cause periodical round-off error in circular movements; the resolution of the latitude and longitude measurements expressed in NMEA format (dddmm.mmmm) corresponds to about 0.142 m.

The PSDs also show the noise characteristics of the GPS measurements, which look similar to a 1/*f*-shaped noise spectrum; above the 1-Hz region, the noise is more white in nature, and the level significantly increases towards the DC area. These 1/*f*-like noises may cause the low-frequency drifting error seen in the time histories of the right side of Figure 9. In general, displacement measurements have been known to be more accurate in low-frequency area than other measurements, such as velocity or acceleration. However, this view may not be valid for displacement measurement using the single-frequency low-cost GPS receivers; the more dominant noises exist in the lower frequency region.

Another observation was made in the time and frequency domains. As shown in the right of Figure 9, the drift components of the signal, which are noise, seem to be quite random and uncorrelated. The PSD diagrams support this observation; the PSD of the average of the four GPS measurements showed lower noise levels (thick black lines in Figure 10), averaging the four time histories resulted in a 6 dB decrease in the noise level over the entire frequency range. The cross PSD (CPSD) of two signals also provides an indication of the uncorrelation of the signal drift. The CPSD of GPS-2 and GPS-4, for example, showed lower noise levels than auto PSD of each GPS measurement (Figure 11).

3.4. GPS signal simulation

On the basis of the previous observation made from Figures 10 and 11, 1/*f*-like artificial noise is used to better understand the characteristics of the low-cost GPS modules and simulate their performance. Many researchers have previously tried to identify these noise characteristics and simulate them, considering numerous GPS noise sources [22–24]. In this study, however, only the statistical characteristics of the noise are of interest; consideration of specific effects of individual noise sources is not sought.

Passing white noise through a filter can easily produce the 1/*f*-like shaped noise. In this study, the $1/f^{\alpha}$ power law noise model is used [25]. In a discrete representation, the resulting spectrum has the form of

$$S_d(f) = Q_d \Delta t^{1-\alpha} / (2\pi f)^{\alpha}, \tag{1}$$

where Q_d is the variance of the input white noise. The transfer function of the $1/f^{\alpha}$ AR filter has the form of

$$H(z) = \frac{1}{a_0 + a_1 z^{-1} + a_2 z^{-2} + a_3 z^{-3} \ldots}, \tag{2}$$

where $z = e^{j2\pi f \Delta t}$ and the filter coefficients for this are

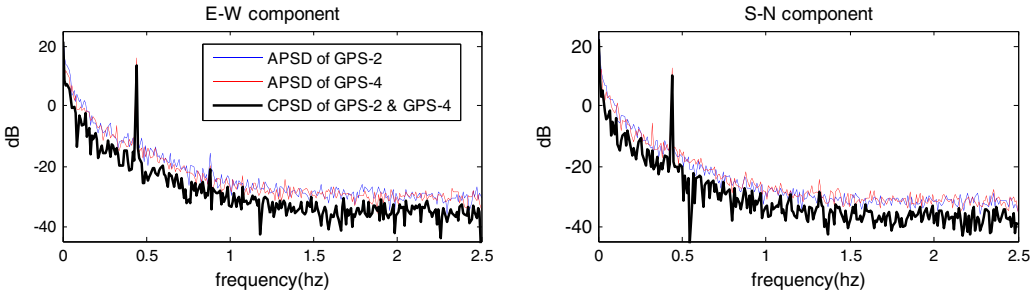

Figure 11. PSDs and CPSD of the GPS-2 and GPS-4 measurements in E/W direction (left) and S/N direction (right): 1.0 m radius and 2.3 s period.

DOI: 10.1002/stc

$$a_0 = 1$$
$$a_k = \left(k - 1 - \frac{\alpha}{2}\right) \cdot \frac{a_{k-1}}{k}, \quad k = 1,\ 2,\ 3.... \tag{3}$$

A sinusoidal wave of 0.43 Hz was generated and then combined with the $1/f^{\alpha}$-shaped white noise to simulate the GPS measurement. A round-off error of 0.142 m, corresponding to the previously mentioned quantization error, is introduced to see if additional frequency peaks appear in the PSD diagram. Figure 12 shows the time histories and PSDs of the simulated GPS measurements. In total, 100 GPS measurements are simulated; one of the typical time histories and the simulation procedure are shown on the left of Figure 12 and their PSDs on the right.

As shown in Figure 12, the spectrum of the simulated noise has the mentioned 1/*f*-like form (right). The time history shows a drift noise, mainly because of more energy in the low-frequency area (left), as seen in the actual measurements in Figures 10 and 11. The round-off error introduced in the sinusoidal motions gives rise to extra peaks in the PSD, as expected (see the right of Figure 12); although not shown here, without the round-off error, there were no additional frequency peaks. Also, the noise reduction effects were observed when the simulated GPS signals were averaged (see the right bottom of Figure 12). Because the simulated GPS noises are based on uncorrelated white noise, the uncorrelated noises should be averaged out during the averaging process. Through the averaging process of four simulated GPS signals, around a 6 dB noise reduction effect was observed, which is similar to the phenomenon seen in actual data (Figure 10). The averaging process of 100 signals created additional noise reduction, in which the PSD of the averaged signal approaches the PSD of the sinusoidal signal (purple line in the right of Figure 12), indicating the potential of utilizing a dense array of low-cost GPS sensors.

3.5. Displacement amplitude change over time

In the dynamic tests, the radius of the circular movements was 1.0 m. However, long-term records spanning 30 min showed lower amplitudes than the expected value. To better identify the characteristics of the measured GPS signals without noise, the time history data shown in Figure 9 were band-pass filtered with the passband of 0.4–0.5 Hz. As shown in Figure 13, the band-pass filtered signals showed an amplitude that was about half of the actual value; moreover, the amplitudes changed both over time and over different GPS units. The RMS values of the ratio between the GPS measurements and the expected value were 0.43 for the E/W direction and 0.39 for the N/S direction for the average of four GPS modules; they were less than 1 and even had a different value in each of the directions.

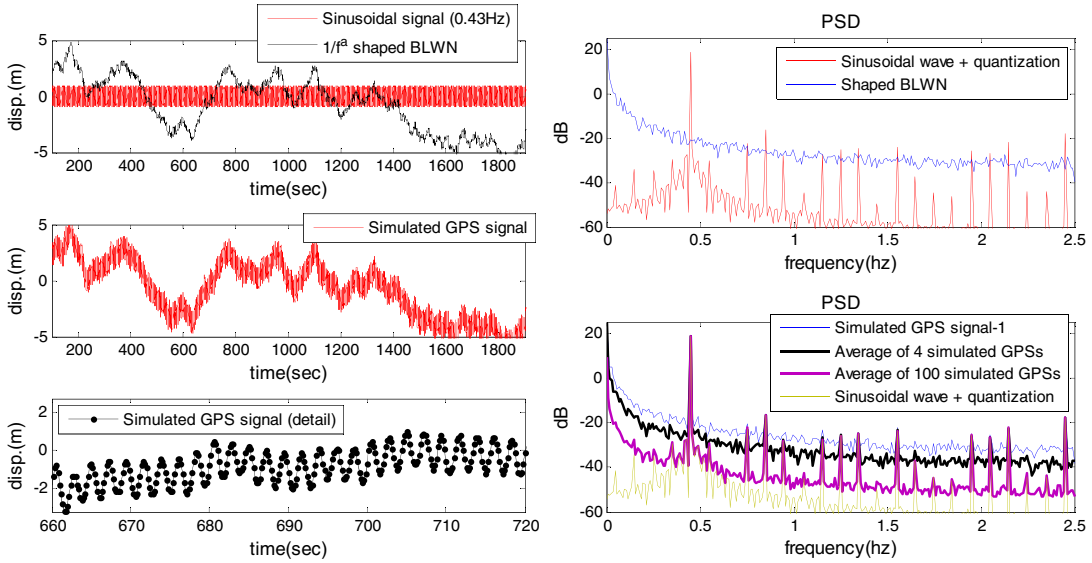

Figure 12. Time histories (left) and PSDs (right) of simulated GPS measurements.

DOI: 10.1002/stc

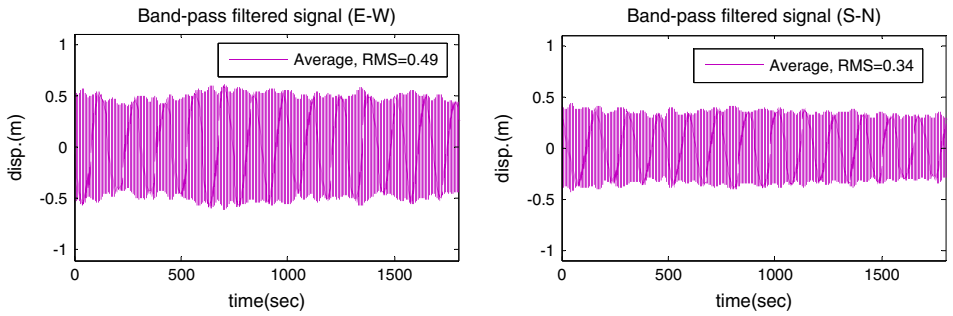

Figure 13. Bandpass filtered time history: average of four GPS measurements, E/W data (left) and S/N data (right).

The amplitude variation phenomenon also has been reported in a dual-frequency GPS testing [20]. The measured displacement amplitudes using dual-frequency RTK GPS receivers (Leica GMX902) fluctuated over time; the RMS values of the ratio between the GPS measurement and the expected value differ (RMS = 0.85–1.2) between different frequencies and different amplitudes, although the errors were the order of sub-centimeters. For the low-cost GPS sensors, the amplitude variation phenomenon seems more severe. More testing results with different amplitude and frequency combinations are discussed in the following section.

For the directional difference of the RMS values of measurement amplitude, one of the main reasons may be attributed to the uneven GPS satellite distribution across the sky in mid-latitude areas [26,27]. Because of the 55° inclination of satellite orbits, no observation is possible in the northern sky quadrant. Figure 14 shows the satellite sky view on the roof of the NCEL building at Illinois (88°15′N, 40°3′W) during 24 h and also the large hole having no satellite traces in the northern sky area. Such a satellite sky distribution would result in worse accuracy in the N/S direction than in the E/W direction, as shown in Figure 13. Ayers *et al*. [28] found a similar phenomenon for the GPS accuracy difference between the E/W and S/N directions; the standard deviation of GPS errors in the S/N direction was higher than in the E/W direction. Wu *et al*. [27] studied the directional accuracy of L1 C/A code-based GPS by investigating the difference in east DOP and north DOP; the north DOP was observed to be much higher than the east DOP, particularly in mid-latitude areas, because of the poor satellite distribution in the northern sky quadrant. For this reason, in the following dynamic test, only the E/W component of the measurement will be considered.

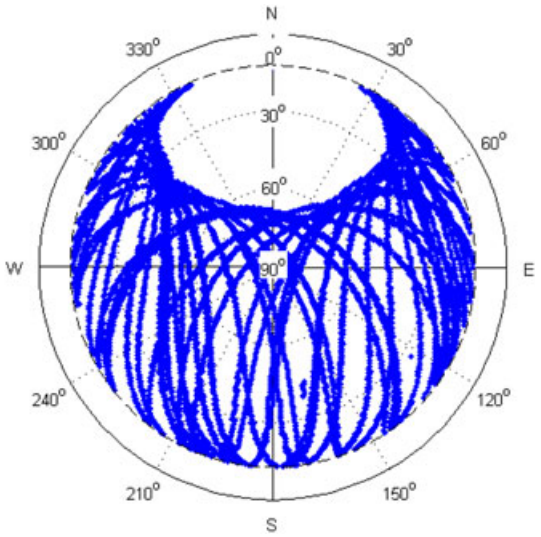

Figure 14. Satellite sky view on the NCEL building at Illinois on May 15, 2011 (24-h duration).

DOI: 10.1002/stc

4. PARAMETRIC DYNAMIC GPS TESTING

To evaluate the performance of the low-cost GPS receivers at different frequencies and displacement amplitudes, parametric dynamic tests were carried out for various combinations of frequencies and amplitudes by changing the rotational speed of the rotor blade and moving the GPS locations along the wooden rotor blade. In this test, six different amplitudes, 0.25, 0.5, 0.75, 1, 1.5, and 2 m, and five different rotational frequencies, 0.098, 0.195, 0.215, 0.461, and 0.68 Hz were used, whereas the other sensing parameters remained unchanged from the previous dynamic tests. The wooden rotor blade was extended to have a 2-m length from the center of rotation.

Because the generated data are too extensive to include in this paper, only one of typical sets of measurements is plotted in Figures 15–17 (the 0.215 Hz rotational frequency test). Figure 15 shows the time histories of measured displacements for the six different amplitudes, which are the average of the data from four Gms-u1LP GPS sensors. Figure 16 shows the PSDs of the measurements; to show the noise reduction effect by averaging process, one of the PSDs of four GPS data is compared with the PSD of the averaged data. Figure 17 shows the band-pass filtered time histories.

As the rotational radius of the GPS sensors changed from 0.25 to 2 m, obvious differences in the measured displacement amplitudes were observed (Figure 15). This observation is even clearer in Figure 17, which shows the band-pass filtered signal; the larger the radius of rotation was used, the larger the displacement amplitudes were measured.

The PSDs for different amplitudes clearly show the corresponding rotational frequency peak at 0.215 Hz, even for the 0.25 m amplitude case (Figure 16). The frequency peak magnitudes for different amplitude cases are different. In the frequency domain, the low-cost GPS sensors showed satisfactory performance. However, as the amplitude becomes smaller, it becomes more contaminated and affected by the low-frequency drift noises. Also, the additional peaks in the PSDs, which should not be there, appeared as expected; the periodical round-off error in the cyclic rotational movement may be the reason, as simulated in Figure 12.

Figure 18 shows the RMS values of the ratio between the measured amplitudes and the expected amplitudes at different rotational frequencies and different displacement amplitudes. Even though further validation is required to draw a conclusion, a trend can be confirmed by similar behaviors for tests with different cases. As shown in Figure 18, it is observed that as the rotation amplitude increases, the closer the RMS value is to 1 (left), and as the rotational frequency decreases, the closer the RMS value is to 1 (right).

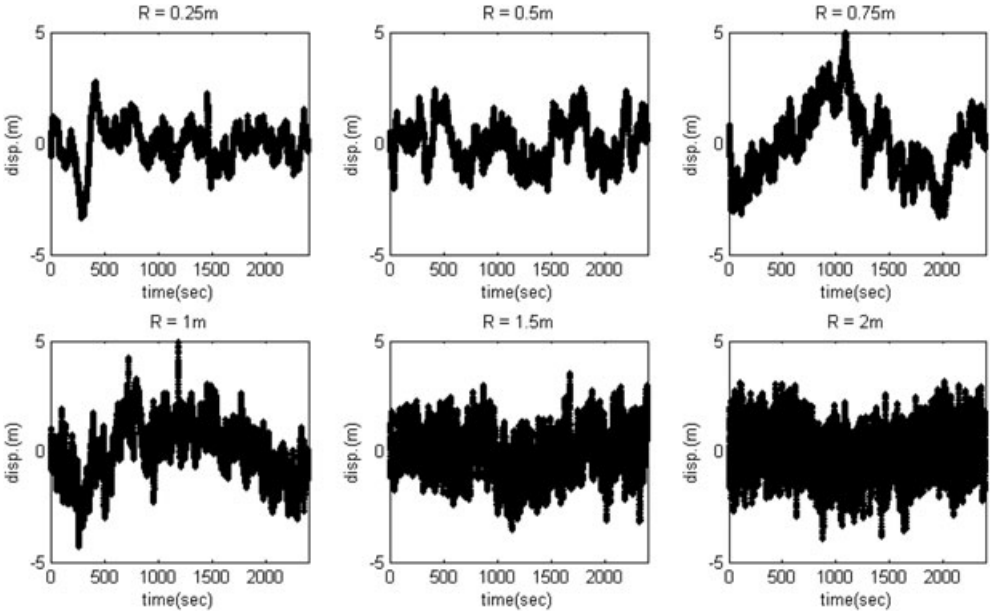

Figure 15. GPS displacement time histories for six different amplitudes at 0.215 Hz (average of four GPS measurements).

DOI: 10.1002/stc

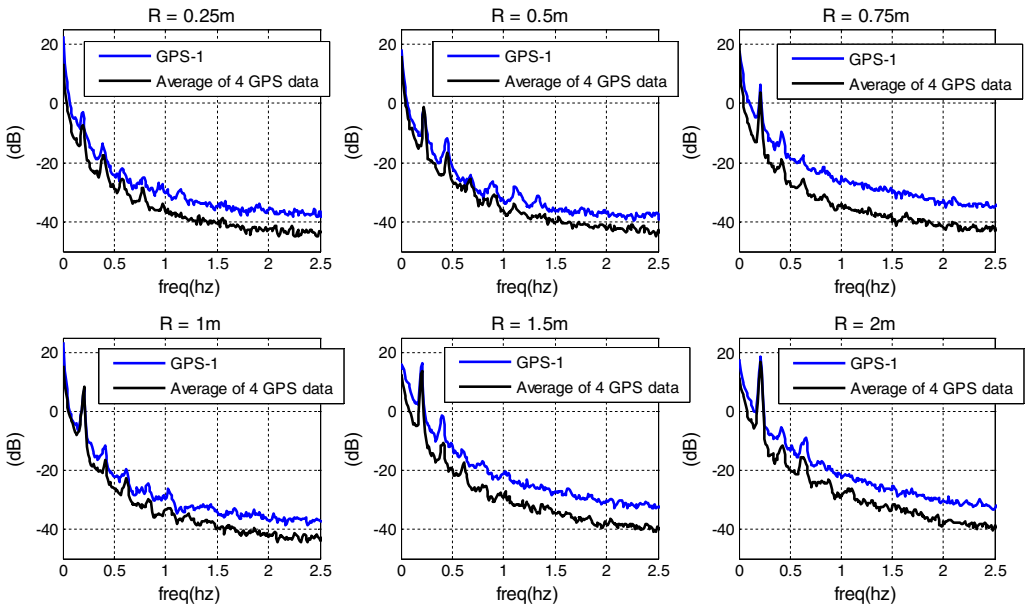

Figure 16. GPS displacement PSDs for six different amplitudes at 0.215 Hz.

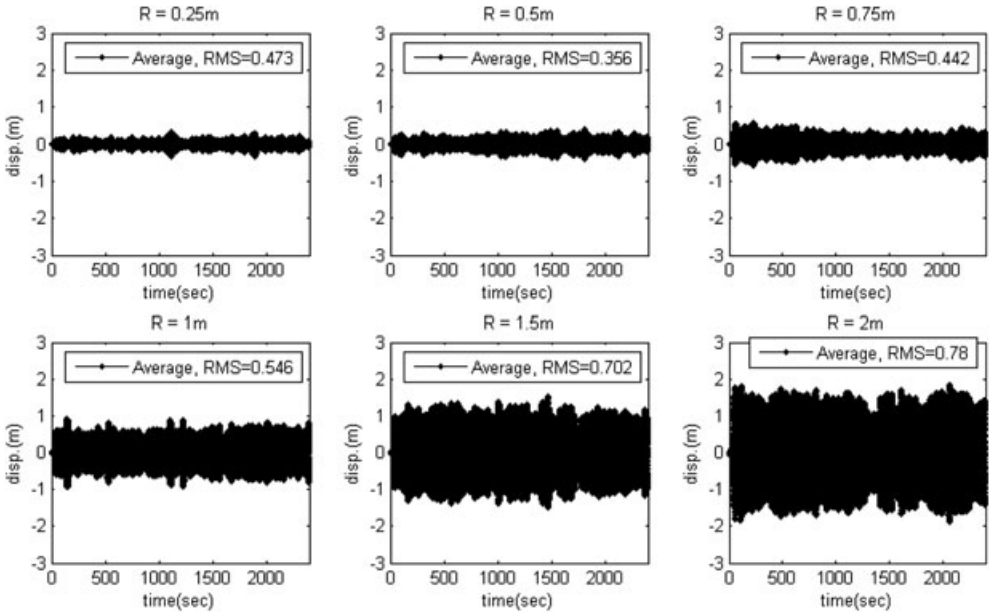

Figure 17. Bandpass filtered GPS time histories for six different amplitudes at 0.215 Hz (average of four GPS measurements).

For the lowest rotational speed of 0.098 Hz, the measurements were contaminated with much low-frequency noise. The RMS values for the 0.098 Hz case, except the $R = 0.25$ m case, were generally close to 1 (green line in the left of Figure 18); however, it was because the noise floor in low-frequency range is too high (1/*f* shape). Even for the 1-m amplitude case, data were overwhelmed by the noise (Figure 19, middle); the amplitude of the frequency peak at 0.098 Hz is small because of high-level noise in the low-frequency range. The higher frequency cases (greater than 0.2 Hz), on the other hand, showed consistently reasonable results (Figure 18, left); the larger amplitude cases yielded more accurate RMS values.

DOI: 10.1002/stc

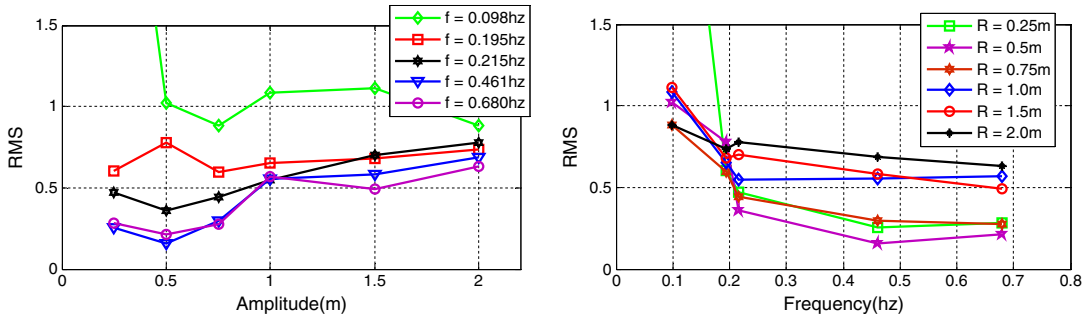

Figure 18. RMS value changes of measured displacement amplitude in different amplitudes (left) and different frequencies (right).

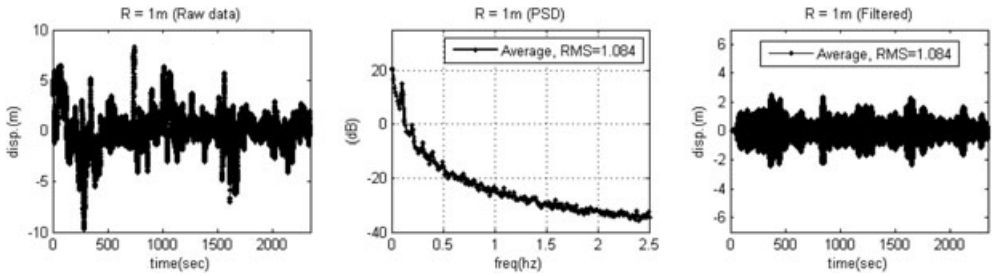

Figure 19. GPS measurement with 1 m amplitude and 0.098 Hz frequency (average of four GPS measurements): raw time histories data (left), PSD (middle), and band-pass filtered data (right).

As for the effect of rotational frequencies on the performance of the GPS receivers, (Figure 18, right), the data showed that better accuracies were present at lower frequencies; the GPS modules better caught the rotational movements at lower speeds. According to the manufacturer of the Gms-u1LP GPS receivers, GlobalTop, this kind of single-frequency GPS contains a function that filters erratic movements in order to obtain better tracking, which is usually used to optimize the receivers for car or pedestrian navigation purposes. Because the GPS sensors on the rotational blade recognize a change in direction each time the position is sampled, as the rotational speed increases, the directional angle change also increases; this could be recognized as the erratic change by the GPS receivers, so long as the angle change is larger than a certain threshold. Of course, this sort of filtering technique will undoubtedly lead to degradation in positioning accuracy in such rotational movements.

5. CONCLUSIONS

The feasibility of low-cost single-frequency GPS receivers for SHM applications has been investigated in this paper. To understand the potential of using the low-cost GPS receivers, diverse static and dynamic experimental tests have been performed. Also, simulated GPS data have been used and compared with real measurements to figure out the GPS noise characteristics.

In the static tests, periodic static noise in individual GPS modules over several days was observed, which could be predicted and subtracted from measurements. However, long-term tests using multiple GPS sensors showed that the repeatability of the static data is affected by weather conditions and non-uniform hardware qualities of sensors.

Through the dynamic tests using a horizontal rotor system, low-frequency drift was observed in the GPS measurements, which had a $1/f$ spectrum. Similar to how the electric fish averages signals from many low-resolution skin sensors to extract necessary information, averaging multiple GPS measurements reduced the noise level, consequently making more apparent frequency peaks in PSD; the noise had low correlation, so averaging process could reduce the noise levels, and the CPSD

DOI: 10.1002/stc

of two different GPS measurements and the simulated GPS data confirmed that GPS noises have low correlation.

The ability of the GPS receivers to capture dynamic displacement responses was quite satisfactory. Even at 0.25 m amplitude, oscillations were captured and appeared clearly in frequency domain. However, amplitude fluctuations and lower amplitude than the actual were observed over time. The dynamic tests with various combinations of amplitudes and frequencies showed that the precision depended on the amplitude and frequency of the signal. Furthermore, the displacement measurements at very low frequencies were very noisy because of 1/*f* noise. Also, poor distribution of the GPS satellites in northern sky diminished positioning accuracy in the N/S measurement direction.

In summary, the possibilities and limitations of the low-cost L1 C/A code-based GPS sensors for SHM applications were explored in this study. The very low-frequency range (i.e., lower than 0.2 Hz) was contaminated by the 1/*f*-shaped noise; however, higher-frequency ranges showed quite consistent behavior in frequency domain, which may prove to be useful for dynamic displacement monitoring of mid-scale cable-suspended bridges. Combined use of the dense array of the low-cost GPS as rovers with a high-precision dual-frequency GPS as reference could be a practical solution; such research is currently underway.

REFERENCES

1. Jang SA, Jo H, Cho S, Mechitov KA, Rice JA, Sim SH, Jung HJ, Yun CB, Spencer BF Jr, Agha G. Structural health monitoring of a cable-stayed bridge using smart sensor technology: deployment and evaluation. *Smart Structures and Systems* 2010; **6**(5-6):439–459.
2. Cho S, Jo H, Jang SA, Park J, Jung HJ, Yun CB, Spencer BF Jr, Seo J. Structural health monitoring of a cable-stayed bridge using smart sensor technology: data analyses. *Smart Structures and Systems* 2010; **6**(5-6):461–480.
3. Kurata M, Kim J, Zhang Y, Lynch JP, Linden GW, Jacob V, Thometz E, Hipley P, Sheng LH. Long-term assessment of an autonomous wireless structural health monitoring system at the New Carquinez Suspension Bridge. *Proc. of SPIE*, San Diego, 2010.
4. Spencer BF, Jo S. Wireless smart sensor technology for monitoring civil infrastructure: technological developments and full-scale applications. *Proc. of ASEM'11+, Seoul* 2011, 4277-4304.
5. Nickitopoulou A, Protopsalti K, Stiros S. Monitoring dynamic and quasi-static deformations of large flexible engineering structures with GPS: accuracy, limitations, and promises. *Engineering Structures* 2006; **28**:1471–1482.
6. Psimoulis PA, Pytharouli S, Karambalis D, Stiros SC. Potential of Global Positioning System (GPS) to measure frequencies of oscillations of engineering structures. *Journal of Sound and Vibration* 2008; **318**:606–623.
7. Psimoulis PA, Stiros SC. Experimental assessment of the accuracy of GPS and RTS for the determination of the parameters of oscillation of major structures. *Computer-Aided Civil and Infrastructure Engineering* 2008; **23**:389–403.
8. Casciati F, Fuggini C. Monitoring a steel building using GPS sensors. *Smart Structures and Systems* 2011; **7**(5):349–363.
9. Ashkenazi V, Dodson A, Moore T, Roberts G. Monitoring the movements of bridges by GPS. *Proc., ION GPS 1997, 10th Int. Technical Meeting of the Satellite Division of the U.S. Institute of Navigation*, Kansas City, Mo., 1997; 1165–1172.
10. Celebi M, Prescott W, Stein R, Hudnut K, Behr J, Wilson S. GPS monitoring of dynamic behavior long-period structures. *Earthquake Spectra* 1999; **15**:55–66.
11. Nakamura S. GPS measurement of wind-induced suspension bridge girder displacements. *Journal of Structural Engineering ASCE* 2000; **12**:1413–1419.
12. Fujino Y, Murata M, Okano S, Takeguchi M. Monitoring system of the Akashi Kaikyo Bridge and displacement measurement using GPS. *Proc. of SPIE, nondestructive evaluation of highways, utilities, and pipelines IV*, 2000; 229–236.
13. Kijewsji-Correa TL, Kareem A, Kochly M. Experimental verification and full-scale deployment of global positioning systems to monitor the dynamic response of tall buildings. *Journal of Structural Engineering* 2006; **132**(8):1242–1253.
14. Watson C, Watson T, Coleman R. Structural monitoring of cable-stayed bridge: analysis of GPS versus modeled deflections. *Journal of Survey Engineering ASCE* 2007; **133**:23–28.
15. Yi TH, Li HN, Gu M. Recent research and applications of GPS based monitoring technology for high-rise structures. *Structural Control and Health Monitoring* 2012 Published online. DOI: 10.1002/stc.1501
16. Knecht A, Manetti L. Using GPS in structural health monitoring. *Proc. of SPIE, Smart Structure and Materials*, SPIE Pub. No. 4328, 2001.
17. Saeki M, Hori M. Development of an accurate positioning system using low-cost L1 GPS receivers. *Computer-Aided Civil and Infrastructure Engineering* 2006; **21**:258–267.
18. Saeki M, Oguni K, Inoue J, Hori M. Hierarchical localization of sensor network for infrastructure monitoring. *Journal of Infrastructure Systems* 2006; **14**(1):15–26.
19. Nelson ME. Biological smart sensing strategies in weakly electric fish. *Smart Structures and Systems* 2011; **8**(1):1–11.
20. Casciati F, Fuggini C. Engineering vibration monitoring by GPS: long duration records. *Earthquake Engineering and Engineering Vibration* 2009; **8**(3):459–467.
21. Haddrell T. Effects on navigation receivers. 2011. (Available from: https://connect.innovateuk.org/c/document_library/get_file?folderId=2652904&name=DLFE-24570.pdf)
22. Genrich JF, Bock Y. Instantaneous geodetic positioning with 10–50 Hz GPS measurements: noise characteristics and implications for monitoring networks. *Journal of Geophysical Research* 2006; **111**(B03403):10.1029/2005Jb003617
23. Amiri-Simkooei AR, Tiberus CCJM, Teunissen PJG. Assessment of noise in GPS coordinate time series: methodology and results. *Journal of Geophysical Research* 2007; **112**(B07413). doi:10.1029/2006JB004913

DOI: 10.1002/stc

24. Borsa AA, Minster JB. Modeling long-period noise in kinematic GPS applications. *Journal of Geodesy* 2007; **81**:157–170.
25. Kasdin NJ. Discrete simulation of colored noise and stochastic process and $1/f^{\alpha}$ power law noise generation. *Proceedings of the IEEE* 2005; **83**(5):802–827.
26. Meng X, Roberts GW, Dodson AH, Cosser E, Barnes J, Rizos C. Impact of GPS satellite and pseudolite geometry on structural deformation monitoring: analytical and empirical studies. *Journal of Geodesy* 2004; **77**:809–822.
27. Wu C, Ayers PD, Anderson AB. Influence of travel direction on GPS accuracy for vehicle tracking. *Transaction of the ASABE* 2006; **49**(3):623–634.
28. Ayers PD, Wu C, Anderson AB. Evaluation of autonomous and differential GPS for multi-pass vehicle racking identification. *ASAE/CSAE Meeting Presentation*, ASAE Paper No. 041061. St. Joseph, Mich.: ASAE, 2004.
29. Kaplan E, Hegarty C. *Understanding GPS Principles and Applications* (2^{nd}edn edn). Artech House: Boston, 2006.
30. Leica Geosystems AG. *GMX 902 User Manual*. Heerbrugg: Switzerland, 2005.
31. GlobalTop Technology Inc. *Gms-u1LP GPS Module Data Sheet*. Tainan, Taiwan, 2010. (Available from: http://www.gtop-tech.com.)

DOI: 10.1002/stc